Procedure for Evaluation of Engine Isolators for Reduced Structure-Borne Noise Transmission

J. F. Unruh*
Southwest Research Institute, San Antonio, Texas

Analytical models of a general aviation aircraft engine, vibration isolators, and engine mount structure are dynamically coupled to an empirical model of the aircraft fuselage for the purpose of developing a structure-borne interior noise transmission model. Laboratory base tests of the aircraft with isolators of various structural properties provided relative isolator performance data for correlation of the analytical model. Results of the study indicate that the frequency-dependent mechanical properties of the isolators play an important role in the transmission of structure-borne noise. The frequency range of interest in the study was up through 1000 Hz.

Nomenclature

C_{S2} = fuselage inertance matrix
F_R = forces applied to engine c.g.
F_{S1} = attach point nodal forces associated with X_{S1}
F'_{S1} = attach point nodal forces associated with X'_{S1}
F_{S2} = nodal forces associated with X_{S2}
F'_{S2} = attach point nodal forces associated with X'_{S2}
i = complex number $\sqrt{-1}$, also index
I = unity diagonal matrix
I_{XX} = engine roll inertia
I_{YY} = engine pitch inertia
I_{ZZ} = engine yaw inertia
k_a = isolator complex axial stiffness
k_r = isolator complex radial stiffness
K = stiffness matrix, in general
K^*_{S2} = fuselage dynamic stiffness matrix
M = mass matrix, in general
M_M = engine mount rigid body mass matrix
M_R = rigid engine mass matrix
P^*_{S2} = firewall force excitation to cabin sound pressure level (SPL) transfer function matrix
q_e = engine mount elastic mode degree of freedom
q_r = engine mount rigid body degree of freedom
Q = engine mount elastic mode eigenvectors
Q_R = engine mount rigid body eigenvectors
T_{cg} = engine c.g. to isolator rigid body transformation
X,Y,Z = Cartesian coordinates
X_I = engine mount interior nodal degrees of freedom
X_R = engine c.g. degrees of freedom
X_{S1} = engine-to-isolator degrees of freedom set
X'_{S1} = engine-mount-to-isolator degrees of freedom set
X_{S2} = fuselage degrees of freedom
X'_{S2} = engine-mount-to-fuselage degrees of freedom set
β = engine mount critical damping ratio
η = material loss factor
$\theta_X,\theta_Y,\theta_Z$ = angular rotations about the Cartesian coordinates
ω = circular frequency
ω_e = engine mount free-free normal mode circular frequency

Presented as Paper 81-1970 at the AIAA 7th Aeroacoustics Conference, Palo Alto, Calif., Oct. 5-7, 1981; submitted Oct. 13, 1981; revision received April 29, 1982.

*Senior Research Engineer, Department of Engineering Mechanics. Member AIAA.

Introduction

OVER the past few years considerable attention has been given to the reduction of interior noise in general aviation aircraft. A majority of the literature in this area has concentrated on reduction of the airborne source by investigating methods for increasing sidewall transmission loss or reducing the propeller signature. The twin engine aircraft has been the major subject of the above referenced work owing to the geometric location of the propeller plane, being in close proximity to the fuselage sidewall. In single engine general aviation aircraft the structure-borne noise component produced by engine vibrations has been shown to be a major source of interior noise.[1] The interior noise spectra shown in Fig. 1 are taken from data presented in Ref. 1, wherein ground tests of a Cessna Model 172 aircraft were carried out using an engine attached/detached test technique to determine the engine induced structure-borne noise contribution. As can be seen by the data given in Fig. 1, engine induced structure-borne noise has significant components up through the 1600-Hz band. For the referenced data which was taken at an engine speed of 2160 rpm, the fundamental propeller tone is in the 80-Hz band, and establishes the major low-frequency component. Responses in the 500-1250-Hz bands establish the major midfrequency contributions.

Improved engine vibration isolation would appear to be a viable noise control measure for the reduction of the structure-borne noise in the single engine aircraft. However, effective application of any noise control measure requires predictive procedures for screening candidate materials and test procedures for verifying the choice of a particular control measure. To this end a program was undertaken to develop the necessary analysis and test procedures to synthesize engine vibration isolation treatments for reduced interior noise transmission. The specific objectives of the program were to 1) develop an analytically based structure-borne noise transmission model for isolator design evaluation, 2) develop a laboratory based test procedure to simulate engine induced structure-borne noise transmission, and 3) test a range of candidate isolators for relative performance data and basic data for transmission model correlation.

In the sections to follow, the procedures used to develop a structure-borne interior noise transmission model of the Cessna Model 172 aircraft are given along with a description of the laboratory based test facility used to obtain isolator relative performance data. Thereafter, comparisons of predicted-to-measured results for various isolator sets are given to verify the transmission model and to point out the modeling detail necessary to insure adequate representation. For additional discussions on the various aspects of the pro-

gram and detailed expressions for the matrix elements used in the transmission model, the reader is referred to Ref. 2.

Transmission Model

Coupled structural acoustic modeling procedures for light-aircraft-type structures have been given some attention over the past few years[3-5]; however, the proposed procedures have not been validated for the higher-frequency region of interest to this study[6] (up through 1000 Hz). The scope of the present study was for the most part limited to investigating the engine mount structure and vibration isolator design and therefore changes to the fuselage/cabin area were not anticipated. For these reasons it was decided that the fuselage/cabin response would be characterized empirically. On the other hand, all components forward of the fuselage firewall were to be modeled analytically so that design variations in these components could be easily incorporated into the system model.

The transmission model was developed using the conventional aircraft global axis system, where X is aft along the centerline of the fuselage, Y is to the pilot's right, and Z is upward for a right-handed system. Each of the four model components: the engine, the vibration isolators, the engine mount structure, and fuselage cabin response, are described in the following sections.

Engine as a Rigid Body

The engine was modeled as a rigid body and is shown schematically in Fig. 2 along with its associated centroidal coordinate set $\{X_R\} = [X, Y, Z, \theta_X, \theta_Y, \theta_Z]$. Also shown are the assumed rigid extension arms to each of the four isolator attach points. At the isolator attach points it is assumed that the 3 translational degrees of freedom are sufficient to model the transmitted engine loads. The rotational degrees of freedom were not represented and therefore no moment carrythrough exists at these points. The degree of freedom set at the isolator attach points is denoted as $\{X_{SI}\} = [X_1, Y_1, Z_1, .., X_4, Y_4, Z_4]$.

The motion at isolator attach point i due to a prescribed engine motion is given by the rigid body transformation defined as

$$\begin{Bmatrix} X_i \\ Y_i \\ Z_i \end{Bmatrix} = [T^i_{cg}] \begin{Bmatrix} X \\ Y \\ Z \\ \theta_X \\ \theta_Y \\ \theta_Z \end{Bmatrix} \tag{1}$$

For the complete attach point coordinate set we may write

$$\{X_{SI}\} = \begin{bmatrix} T^1_{cg} \\ T^2_{cg} \\ T^3_{cg} \\ T^4_{cg} \end{bmatrix} \{X_R\} \equiv [T_{cg}]\{X_R\} \tag{2}$$

The dynamic equations of motion for the rigid engine may be written as

$$[M_R]\{\ddot{X}_R\} = \{F_R\} + [T_{cg}]^T \{F_{SI}\}_R \tag{3}$$

where M_R is the rigid engine diagonal mass matrix comprising $(M,M,M,I_{XX}, I_{YY}, I_{ZZ})$; $\{\ddot{X}_R\}$ are the c.g. accelerations; and $\{F_{SI}\}_R$ are the attach point nodal forces associated with the displacement set $\{X_{SI}\}$. Throughout this paper differentiation with respect to time will be denoted by the dot superscript; thus, for accelerations, the double dot superscripts are employed.

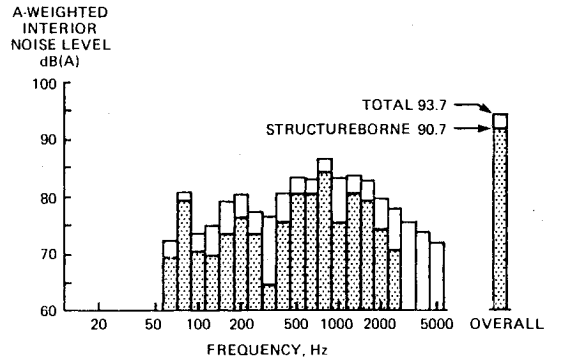

Fig. 1 Structure-borne noise equals airborne noise.

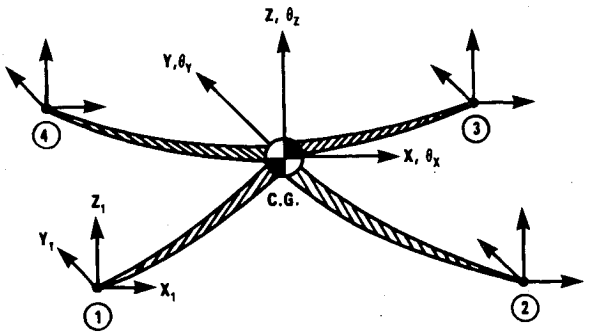

Fig. 2 Engine rigid body and coupling degrees of freedom.

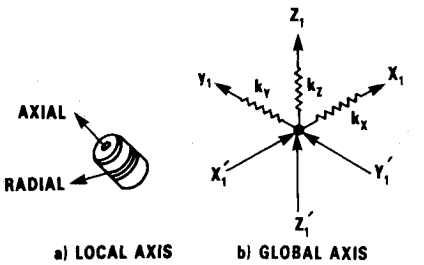

Fig. 3 Vibration isolator degrees of freedom.

Vibration Isolators

The vibration isolators were modeled in their local axis as being independent radial, k_r, and axial, k_a, frequency-dependent springs.

$$k_r = k_r^*(\omega)\,[1 + i\eta(\omega)] \tag{4}$$

and

$$k_a = k_a^*(\omega)\,[1 + i\eta(\omega)] \tag{5}$$

where i is the complex number $\sqrt{-1}$; $k_r^*(\omega)$ and $k_a^*(\omega)$ are the radial and axial spring modulus amplitudes; and $\eta(\omega)$ is the isolator material loss factor. At this point we have for the most part specified harmonic excitation. However, the equations of motion hereafter will still retain their time domain formulations for a consistent representation among all components of the model. The isolators are considered to have an effective dynamic mass equal to their physical mass.

The vibration isolator is schematically shown in Fig. 3 in its local and global axis representation. The degrees of freedom (DOF) associated with the isolators are those on the engine side of the isolator, previously defined as $\{X_{SI}\}$ and a corresponding set on the engine mount side of the isolator, $\{X'_{SI}\}$.

The dynamic equations of motion for the isolators may be written as

$$\begin{bmatrix} M_{VI}^{11} & 0 \\ 0 & M_{VI}^{22} \end{bmatrix} \begin{Bmatrix} \ddot{X}_{SI} \\ \ddot{X}'_{XI} \end{Bmatrix} + \begin{bmatrix} K_{VI}^{11} & K_{VI}^{12} \\ K_{VI}^{21} & K_{VI}^{22} \end{bmatrix} \begin{Bmatrix} X_{SI} \\ X'_{SI} \end{Bmatrix} = \begin{Bmatrix} F_{SI} \\ F'_{SI} \end{Bmatrix}_{VI} \tag{6}$$

where $\{F_{SI}\}$ and $\{F'_{SI}\}$ are the nodal forces associated with the $\{X_{SI}\}$ and $\{X'_{SI}\}$ coordinate sets, respectively. The assembled isolator mass and stiffness matrices, M_{VI} and K_{VI}, reflect the isolator axial alignment being 45 deg to the global Z axis thereby coupling Y-Z motion.

Engine Mount Structure

The engine mount structure is an assemblage of 1.91- and 1.59-cm 4130 steel tubes which form a very strong and lightweight (5.22 kg) carrythrough structure. The engine mount is schematically shown in Fig. 4 with its corresponding coupling degrees of freedom. The coordinate set $\{X'_{SI}\}$ is the coupling degrees of freedom associated with the isolator attach points, and the set $\{X'_{S2}\}$ is associated with the engine-mount-to-fuselage attach points. A finite element model of the engine mount was developed to represent its dynamic characteristics up through 1000 Hz. The model consisted of 72 structural nodes interconnected with 70 elastic beam elements, resulting in a dynamic model with 201 degrees of freedom. The isolator attachment lugs, see Fig. 5, were not modeled in the finite element model. These lugs are modeled as a spring in series with the isolator. The lowest stiffness is in the axial direction with a minimum value of 5.25×10^6 N/m. The local stiffness of the lugs are of interest only in the "rigid" isolator configuration which will be discussed in a following section.

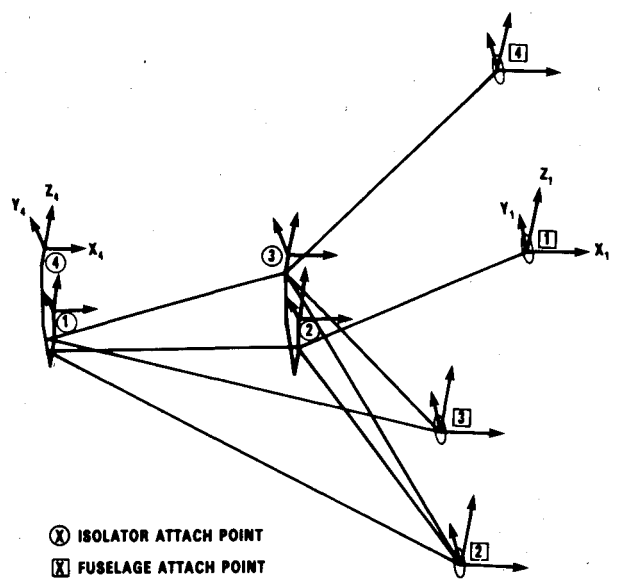

Fig. 4 Engine mount structure with coupling degrees of freedom.

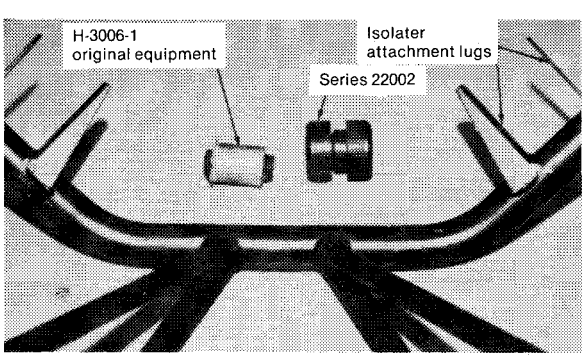

Fig. 5 Vibration isolators and mounting lugs.

Modal synthesis techniques were used to reduce the number of degrees of freedom in the model. The model was expanded in terms of its free-free normal mode responses. A total of 51 normal modes of the free structure exist in the frequency range up to 1000 Hz. In addition to the 51 elastic modes, an additional 6 rigid body degrees of freedom are necessary to completely describe the engine mount response to arbitrary motion. Owing to the high number of elastic mode responses, the elastic modes were band selected in groups of 30 each during the model predictions.

The resulting dynamic equations of motion for the engine mount structure are, in matrix form,

$$\begin{bmatrix} M_M & 0 \\ 0 & I \end{bmatrix} \begin{Bmatrix} \ddot{q}_r \\ \ddot{q}_e \end{Bmatrix} + \begin{bmatrix} 0 & 0 \\ 0 & 2\beta\omega_e \end{bmatrix} \begin{Bmatrix} \dot{q}_r \\ \dot{q}_e \end{Bmatrix} + \begin{bmatrix} 0 & \\ 0 & \omega_e^2 \end{bmatrix} \begin{Bmatrix} q_r \\ q_e \end{Bmatrix} = \begin{bmatrix} Q_{R1}^T \\ Q_{e1}^T \end{bmatrix} \{F'_{SI}\}_M \quad \begin{bmatrix} Q_{R2}^T \\ Q_{e2}^T \end{bmatrix} \{F_{S2}\}_M \tag{7}$$

where M_M is the engine mount rigid body mass matrix; I is a unit diagonal matrix; β is an imposed critical damping ratio for each elastic mode, ω_e is the normal mode frequency; Q_{RI} and Q_{eI}, respectively, are the rigid body and elastic mode components associated with the $\{X'_{SI}\}$ DOF set; Q_{R2} and Q_{e2} are, respectively, the rigid body and elastic mode components associated with the $\{X_{S2}\}$ DOF set; $\{F'_{SI}\}_M$ are the nodal forces at the isolator attach points; $\{F_{S2}\}_M$ are the nodal forces at the fuselage attach points; $\{q_r\}$ are the 6 rigid body DOF; and $\{q_e\}$ is the elastic mode DOF. The nodal motions of the engine mount are related to the rigid body and elastic mode DOF via the normal mode eigenvectors.

$$\begin{Bmatrix} X'_{SI} \\ X'_{S2} \\ X_I \end{Bmatrix} = \begin{bmatrix} Q_{RI} & Q_{eI} \\ Q_{R2} & Q_{e2} \\ Q_{RI} & Q_{eI} \end{bmatrix} \begin{Bmatrix} q_r \\ q_e \end{Bmatrix} \tag{8}$$

For completeness in the above expression, all interior nodal degrees of freedom of the engine mount structure, $\{X_I\}$, have been included. However, the interior set, $\{X_I\}$, is not needed in the transmission model and therefore was not retained.

Aircraft Fuselage and Interior Response

The dynamic characteristics of the fuselage at the engine mount attachment points and the response of selected cabin interior locations were determined by what is generally referred to as point and/or transfer impedance testing. For the problem at hand it would be most convenient to represent the fuselage as a series of coupled spring-like elements wherein mathematically we may write

$$[K^*_{S2}]\{X_{S2}\} = \{F_{S2}\}_F \tag{9}$$

K^*_{S2} is the frequency-dependent dynamic stiffness matrix; $\{X_{S2}\}$ the nodal displacements on the fuselage at the engine mount attach points; and $\{F_{S2}\}_F$ the corresponding nodal forces. The degrees of freedom associated with the firewall are shown in Fig. 6. Again the rotational DOF were not retained at the engine-mount-to-fuselage attach points.

Direct measurement of displacement was not considered to be convenient or reliable for the determination of K^*_{S2}. However, the use of acceleration as a base would allow direct and accurate recording of the inertance at the points of interest for a number of possible forms of excitation. In terms of inertance,

$$\{\ddot{X}_{S2}\} = [C^*_{S2}]\{F_{S2}\}_F \tag{10}$$

where $\{\ddot{X}_{S2}\}$ are the nodal accelerations and C^*_{S2} is the frequency-dependent inertance matrix. Upon inversion of the inertance matrix we obtain the system apparent mass and for harmonic motion $\{\ddot{X}_{S2}\} = -\omega^2\{X_{S2}\}$, which allows formulation of the desired dynamic stiffness matrix in terms of the measurable inertance matrix;

$$[K^*_{S2}] = -\omega^2[C^*_{S2}]^{-1} \tag{11}$$

Sound pressure level (SPL) responses at selected points within the cabin interior, denoted as P1, P2, and P3, are also characterized with respect to the nodal forces $\{F_{S2}\}_F$ as

$$\{P_I\} = [P^*_{S2}]\{F_{S2}\}_F \tag{12}$$

where $\{P_I\}$ are the responses at P1, P2, and P3; and P^*_{S2} is a matrix of firewall force excitation to cabin SPL transfer functions.

Application of a single nodal force, with all other nodes force free, will allow determination of a column of the inertance matrix, C^*_{S2}, by recording all nodal accelerations, and a column of the pressure matrix, P^*_{S2}, by recording all interior pressure responses. A continuous random source was chosen for the present investigation. Data analysis procedures for the random data are straightforward,[8] but rather lengthy. A triaxial accelerometer arrangement was used to simultaneously record orthogonal acceleration responses at a single engine mount attach point along with the input force signal and the three interior SPL responses.

A typical driving point inertance spectrum is given in Fig. 7; the magnitude is given in gravity units per Newton input force. From Fig. 7 we note that the overall response is primarily stiffness-like throughout the major frequency region of interest. The measured spectra showed the fuselage to be dynamically a very symmetric structure, and reciprocity was reasonably well satisfied during the data acquisition process.[2] For use in the analytical model, quasisymmetric off-diagonal terms were averaged to insure reciprocity.

For the bare fuselage interior the sound pressure level transfer function spectra were quite rich in harmonic content. The response at microphone P3 due to excitation at F_{SI} is given in Fig. 8. Microphone P3 is located at the midcabin rear passenger position. The arrow around 64 Hz in the spectrum indicates the response at the cabin fundamental acoustic resonance.

The dynamic stiffness matrices, $[K^*_{S2}]$, and the pressure transfer function matrices, $[P^*_{S2}]$, were developed at 2.0-Hz intervals from 10 to 1000 Hz for characterization of the fuselage. Linear interpolation of the complex matrices allowed continuous representation of these quantities throughout the frequency range of interest.

Component Coupling Procedures

The independent degrees of freedom chosen for the transmission model are the 6 engine rigid body DOF, $\{X_R\}$; the 6 engine mount rigid body DOF, $\{q_r\}$; and the engine mount elastic DOF, $\{q_e\}$. The various component expressions are coupled via force summations at each of the component interfaces: 1) at the rigid engine to isolators,

$$\{F_{SI}\}_R + \{F_{SI}\}_{VI} = 0 \tag{13a}$$

2) at the isolators to engine mount,

$$\{F'_{SI}\}_{VI} + \{F'_{SI}\}_M = 0 \tag{13b}$$

3) at the engine mount to fuselage,

$$\{F_{S2}\}_M + \{F_{S2}\}_F = 0 \tag{13c}$$

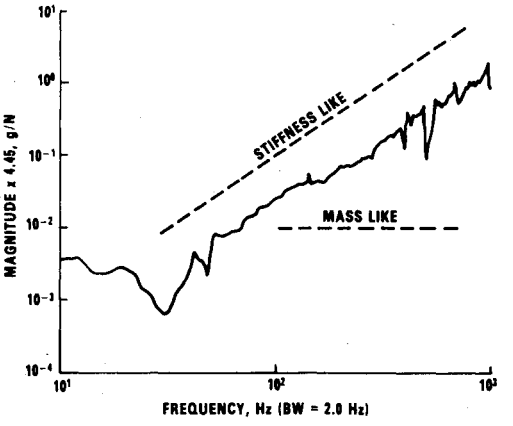

Fig. 7 Fuselage driving point inertance at X_1.

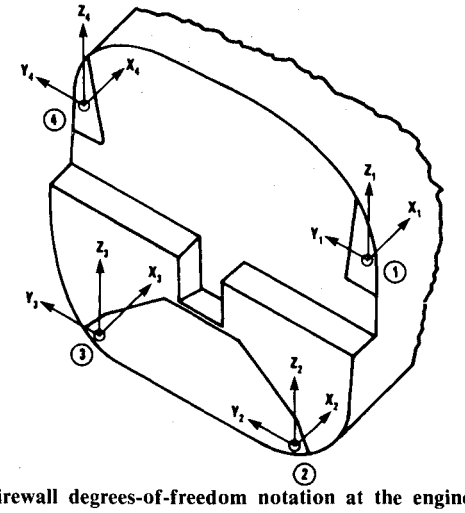

Fig. 6 Firewall degrees-of-freedom notation at the engine mount attach points.

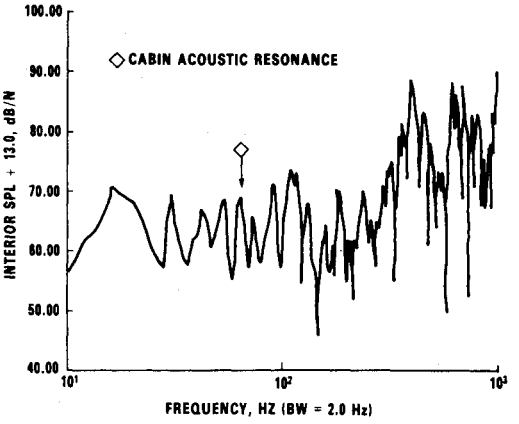

Fig. 8 Fuselage sound pressure level transfer function, input at X_1, response at P3.

Table 1 Engine mass properties

Item	Measured parameters	Designed parameters
M, kg	170	170
I_{XX}, kg m^2	1.756	1.747
I_{YY}, kg m^2	7.901	8.369
I_{ZZ}, kg m^2	14.338	8.837
X_{cg}, m	−0.522	−0.522
Y_{cg}, m	0	0
Z_{cg}, m	0.070	0.070

Table 2 Isolator mechanical properties

Isolator configuration	Radial stiffness k_r^*, N/m	Axial stiffness k_a^*, N/m
R1—Rigid	1.75×10^7	1.75×10^7
R5—R1 + mount lug	1.75×10^7	5.25×10^6
OA—Original equipment	6.02×10^6	4.64×10^5
AA—Soft rubber	2.83×10^5	2.19×10^5

Compatibility of displacements at each of the component interfaces is implied via the use of consistent nodal displacements throughout the component models. The resulting fully coupled system of equations take the form

$$\begin{bmatrix} M_{11} & 0 & 0 \\ 0 & M_{22} & M_{23} \\ 0 & M_{32} & M_{33} \end{bmatrix} \begin{Bmatrix} \ddot{X}_R \\ \ddot{q}_r \\ \ddot{q}_e \end{Bmatrix} + \begin{bmatrix} 0 & 0 & 0 \\ 0 & 0 & 0 \\ 0 & 0 & 2\beta\omega_e \end{bmatrix} \begin{Bmatrix} \dot{X}_R \\ \dot{q}_r \\ \dot{q}_e \end{Bmatrix} + \begin{bmatrix} K_{11} & K_{12} & K_{13} \\ K_{21} & K_{22} & K_{23} \\ K_{31} & K_{32} & K_{33} \end{bmatrix} \begin{Bmatrix} X_R \\ q_r \\ q_e \end{Bmatrix} = \begin{Bmatrix} F_R \\ 0 \\ 0 \end{Bmatrix} \tag{14}$$

where detailed expressions for the various matrix elements are given in Ref. 2. Upon specification of a set of forces applied at the engine c.g., the resulting interior pressures are determined from

$$P_I = [P_{S2}^*]\,[K_{S2}^*]\,[Q_{R2}\,|\,Q_{e2}] \begin{Bmatrix} q_r \\ q_e \end{Bmatrix} \tag{15}$$

The above complex valued expressions were programed for solution in FORTRAN IV-Plus on a DEC PDP 11/70 computer.

Experimental Program

Test Facility

The 1963 Cessna model 172 single engine aircraft used in the previously referenced source identification ground tests was also employed in the present investigation. In the previous studies, engine attached/detached tests were carried out to determine the structure-borne noise component. The structure-borne noise levels were determined by subtracting the airborne noise, which was obtained during the engine detached tests, from the engine attached spectra. The subtraction of the airborne component worked quite well since both source components were of near equal strength. However, it was realized that if moderate reductions in structure-borne noise were obtained, the engine running test facility would not yield accurate measures of structure-borne noise levels. This was the major reason for developing a laboratory based test facility. The simulation of engine excitation would be supplied by electrodynamic shaker excitation applied to the engine. After preliminary laboratory tests it was felt that shaker excitation of the engine could be harmful to the engine bearings unless the propeller was continuously rotated during the tests. It was also desirable to have well-defined engine mass properties for development of the analytical model and a mechanically convenient means of varying engine isolator properties. For these reasons a dummy engine mass was designed for the laboratory test facility.

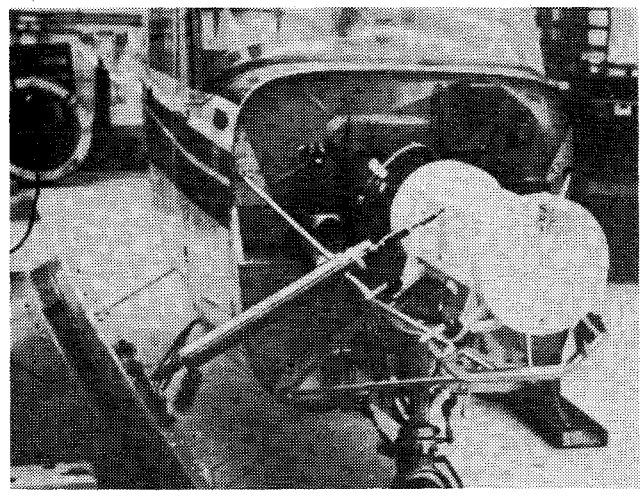

Fig. 9 Dummy engine and test setup.

The dummy engine mass properties were designed to meet the primary mass properties of the actual engine, which were determined from a series of static weight measurements to determine the engine center of gravity and a series of swing tests to measure principal inertias. In Table 1, the actual engine measured mass properties and the dummy engine design calculated mass properties are listed.

The design of the dummy engine allowed direct use of the existing engine mount frame and the incorporation of a series of engine vibration isolators with varying mechanical properties in addition to the original equipment isolators (see Fig. 5). The original equipment isolator, OA, was adapted to the dummy engine via a pair of ring collars to pick up engine loads in the axial direction. A rigid (steel), R1, set of isolators, duplicating the soft rubber, AA, Series 22002 isolator dimensions, was also manufactured to provide a baseline configuration. The static isolator properties were obtained from the manufacturer's product literature and are listed in Table 2. For the purposes of maintaining numerical stability in the solution procedures, the "rigid" isolator stiffness was set to a finite value. Adjustment for local engine mount lug stiffness for the rigid isolator is listed as configuration R5. The baseline values for the material loss factor (η) for the isolators were taken to be 0.10; specific loss factor data were not given in the product literature.

The wings, empennage, and interior trim were removed from the test aircraft during previous investigations. A 1.27-cm plywood bulkhead was installed at body station 108, which separated the cabin area from the fuselage aft tail cone. This bulkhead replaced the standard interior trim, which was a thin plastic panel with molded stiffeners. In this configuration the cabin was most sensitive to structure-borne noise transmission and provided a maximum signal-to-noise ratio for the acoustically untreated laboratory environment.

Engine excitation was provided by a 7100-N Unholtz Dickie electrodynamic shaker which could be attached directly to the dummy engine at various points, resulting in several loading

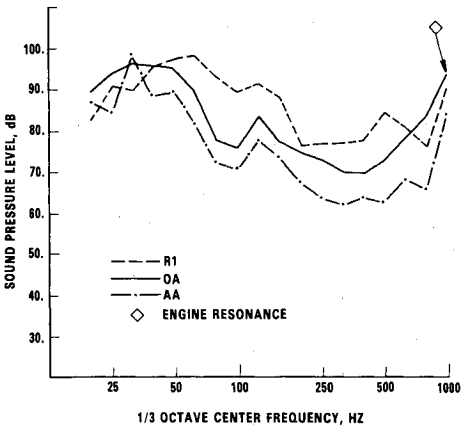

Fig. 10 Measured peak SPL transfer function response at P1, load case 2, reference 89-N rms.

configurations. Load case 2 allowed for simulation of engine torque oscillations. In Fig. 9, the test facility is shown in the load case 2 configuration. The engine c.g. force and moments corresponding to load case 2 are $F_y = -0.875\ F_S$, $F_Z = 0.485\ F_S$, and $M_X = 0.212\ F_S$, where F_S is the shaker input force. For all data presented in this paper, F_S was set at 89-N rms.

A load cell was attached directly to the engine at the shaker attach points to provide for input force control. Three microphones were located within the aircraft cabin: P1 at the pilot's right ear position, P2 at the copilot's left ear position, and P3 midcabin at the passenger's ear level to record interior SPL response.

An amplitude servo/monitor driven by a sweep oscillator provided a signal for a constant harmonic input force. The oscillator was swept from 10 up through 1000 Hz at a rate of 2 Hz/s, which was the fastest sweep rate possible without loss of peak response in the low-frequency region. The interior microphone signals were input into a tracking filter set on a 5.0 Hz bandwidth. The outputs of the tracking filter were routed to X-Y recorders to obtain transfer function data. A Fast Fourier Transform (FFT) computing spectrum analyzer was also used to record one-third-octave peak SPL responses of the interior microphones.

The sound pressure level data presented herein are referenced to $p_r = 2 \times 10^{-5}$ N/m^2.

Data Correlations

The test aircraft in flight operates at an engine speed ranging from 2100 to 2700 rpm. The resulting engine excitation spectra consist of engine ½-rpm harmonics of multiples ranging from 17.5 to 22.5 Hz. The resulting combined operational excitation spectra are therefore dense beyond 70 Hz. The probability of coincidence of an engine harmonic with peaks in the measured structure-borne noise transfer function spectra would be high for normal flight conditions. With this in mind, the sound pressure level transfer function data were analyzed with a FFT analyzer set on the peak capture mode for one-third-octave resolution. A plot of the resulting SPL transfer function data at P1 for load case 2, and isolator configurations R1, OA, and AA are given in Fig. 10. The presentation of the data in terms of peak one-third-octave transfer function level greatly improves the interpretation of the relative performance of the various isolators. The dramatic increase in SPL response in the 1000-Hz band is due to a 970-Hz dummy engine resonant bending response. Likewise, the interpretations of the level of correlation between predicted and measured results were considerably enhanced with presentation of the one-third-octave spectra data, as is shown by the spectra given in Fig. 11. As previously discussed, the engine-mount-to-isolator lug compliance was not modeled in the engine mount component but rather represented as compliance in series with the isolator. The effect of local lug compliance is represented as a

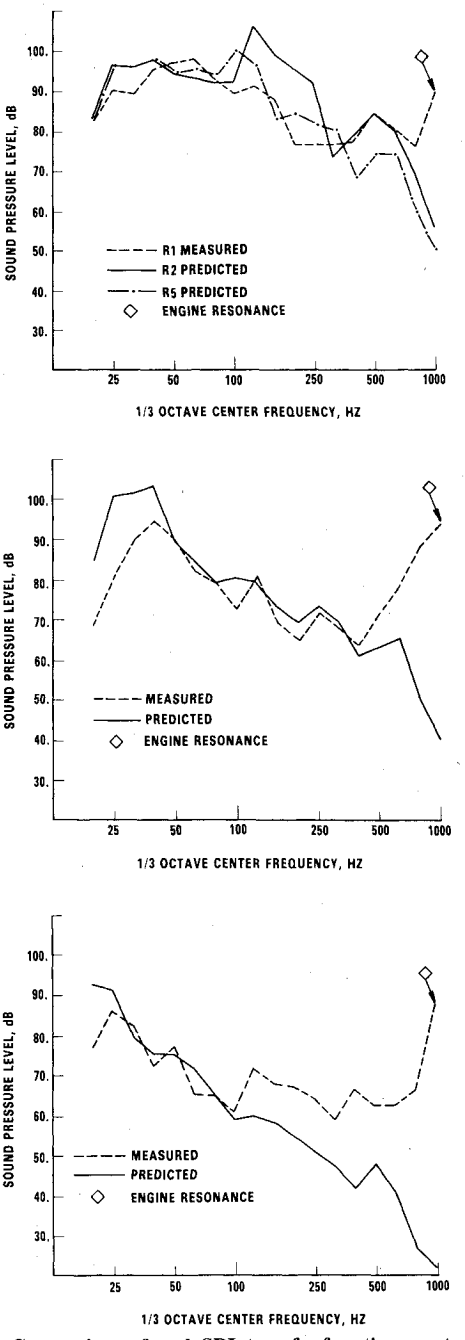

Fig. 11 Comparison of peak SPL transfer function spectra at P1.

reduction in rigid isolator stiffness, as shown by isolator configuration R5 given in Table 2. Corresponding predicted spectra are given in Fig. 11a and, as can be seen, taking into account the local lug stiffness, greatly improved the "rigid" isolator predictions in the region from 100 to 300 Hz. For the compliant isolator predictions, the lug stiffness, of course, had little effect owing to the in series arrangement of the two compliances.

It is felt that the "rigid" isolator test results are reasonably well predicted throughout the frequency region of interest, with the only exception being the response dominated by the dummy engine elastic mode which was not included in the transmission model. This being the case, the discrepancies in the predicted results for the compliant isolator tests are attributed to insufficient representation of the isolators themselves.

In Fig. 12, the effects of varying the isolator material loss factor η from the nominal value of 0.10 up to 1.0 are given. As expected, changes in isolator damping mainly affected the response at the engine fundamental support frequency.

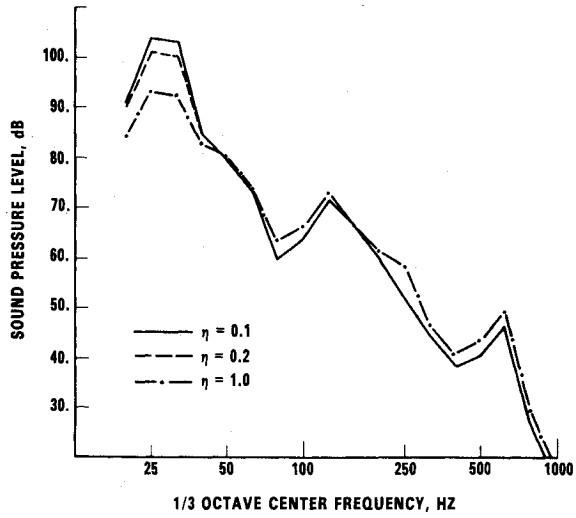

Fig. 12 Predicted effects of isolator damping on peak SPL transfer function spectra at P1, load case 2, configuration AA, reference 89-N rms.

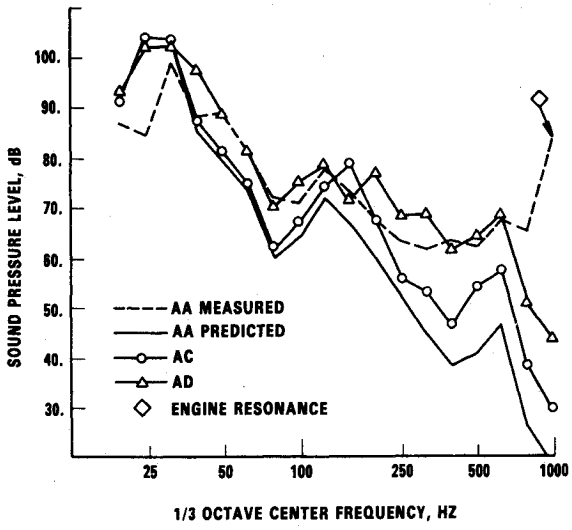

Fig. 13 Effects of isolator stiffness variation on peak SPL transfer function spectra at P1, load case 2, reference 89-N rms.

However, it should be noted that doubling the isolator material loss factor did not decrease the interior response by 6 dB at the engine support frequency, but more on the order of from 2.5 to 3.0 dB were realized. This is due to other system damping being present, such as interior absorption or cabin radiation losses which are reflected in the fuselage dynamic stiffness.

The rapid fall-off of predicted interior SPL transfer function response in the higher-frequency region for the OA and AA isolators as compared to the measured data is attributed to the frequency dependence of the isolator material properties. The exact material properties of the isolators were not known; only their static deflection characteristics were known with a reasonable degree of certainty. Results of a study to determine the degree of frequency dependence of the isolator material properties necessary to bring the model predictions up to the measured results are shown in Fig. 13. In Fig. 13 one-third-octave peak SPL transfer function measured data are compared to predictions for 1) configuration AA, wherein the nominal static isolator properties are used; 2) configuration AC, wherein the isolator stiffness increased linearly to five times its static value in the frequency range from 10 to 1000 Hz; and 3) configuration AD, wherein a linear increase to 25 times the static stiffness occurs over the predicted frequency range. The results given in Fig. 13 show that the variation in isolator stiffness with frequency is a strong parameter for correlation to the measured data.

For the sake of completeness it should be pointed out that an in-depth study of the engine mount structure was also carried out during the program. Owing to its extremely lightweight/high-strength design, the engine mount dynamic response did not greatly influence the overall transmission characteristics of the system.[2]

Concluding Remarks

Analytical models of the simulated engine, vibration isolators, and engine mount structure were coupled to an empirical model of the fuselage for the purpose of developing a structure-borne interior noise transmission model of a test aircraft. From analysis of interior SPL transfer function data obtained from laboratory based tests for a series of isolators with varying mechanical properties, and comparison of the data to predicted transmission levels, the following observations were made.

1) The elastometric isolators do not appear to operate as constant property single-degree-of-freedom systems with respect to noise isolation. Noise isolation beyond approximately 150 Hz levels off and appears to decrease somewhat above 600 Hz.

2) The frequency dependence of the isolator material properties appears to play an important role in the transmission of structure-borne noise in the mid- to high-frequency region of the spectrum. Isolator stiffness is a strong parameter, while isolator damping is a much weaker parameter.

3) For the test aircraft, moderate changes to the lightweight/high-strength engine mount structure did not effect the transmission phenomena.

4) The modeling procedures used appear to be adequate to judge the relative performance of candidate isolators for the purpose of retro-fit isolator design if the mechanical properties of the isolators are known.

Acknowledgments

This investigation was supported by NASA Langley Research Center under Contract NAS1-14861. Assistance by Dennis C. Scheidt during laboratory data acquisition is gratefully acknowledged.

References

[1]Unruh, J.F., Scheidt, D.C., and Pomerening, D.J., "Engine Induced Structural-Borne Noise in a General Aviation Aircraft," NASA CR-159099, Aug. 1979.

[2]Unruh, J.F. and Scheidt, D.C., "Engine Isolation for Structure-Borne Interior Noise Reduction in a General Aviation Aircraft," NASA CR-3427, May 1981.

[3]Dowell, E.H., Gorman, G.F. III, and Smith, D.A., "Acoustoelasticity: General Theory, Acoustic Natural Modes and Forced Response to Sinusoidal Excitation, Including Comparisons with Experiment," *Journal of Sound and Vibration,* Vol. 52, No. 4, 1977, pp. 519-542.

[4]Unruh, J.F., "Finite Element Subvolume Technique for Structural-Borne Interior Noise Prediction," *Journal of Aircraft,* Vol. 17, June 1980, pp. 434-441.

[5]Vaicaitis, R., "Noise Transmission Into a Light Aircraft," *Journal of Aircraft,* Vol. 17, Feb. 1980, pp. 81-86.

[6]Unruh, J.F., "Structural-Borne Noise Prediction for a Single Engine General Aviation Aircraft," AIAA Paper 80-1037, June 1980.

[7]Craig, R.R. Jr. and Chang, C-J., "Substructure Coupling for Dynamic Analysis and Testing," NASA CR-2781, Feb. 1977.

[8]Bendat, J.S. and Piersol, A.G., *Random Data: Analysis and Measurement Procedures,* Wiley-Interscience, New York, 1971.